Dynamics of a linear system coupled to a chain of light nonlinear oscillators analyzed through a continuous approximation

Simon Charlemagne, Alireza Ture Savadkoohi, Claude-Henri Lamarque

Dynamics of a linear system coupled to a chain of light nonlinear oscillators analyzed through a continuous approximation

S. Charlemagne*, A. Ture Savadkoohi, C.-H. Lamarque

Univ Lyon, École Centrale de Lyon, ENISE, ENTPE, CNRS, Laboratoire de Tribologie et Dynamique des Systèmes LTDS UMR5513, F-69518, VAULX-EN-VELIN, France

Abstract

The continuous approximation is used in this work to describe the dynamics of a nonlinear chain of light oscillators coupled to a linear main system. A general methodology is applied to an example where the chain has local nonlinear restoring forces. The slow invariant manifold is detected at fast time scale. At slow time scale, equilibrium and singular points are sought around this manifold in order to predict periodic regimes and strongly modulated responses of the system. Analytical predictions are in good accordance with numerical results and represent a potent tool for designing nonlinear chains for passive control purposes.

Keywords: Nonlinear chain, Continuous approach, Vibratory energy, Time multi-scales method, Passive control

1. Introduction

Study of vibratory energy mitigation through addition of light structures was first studied in the early 1910's with the invention of what is usually referred to as Tuned Mass Damper (TMD) [1]. This linear added oscillator is tuned to a special frequency in order to oscillate in the opposite phase of the main system to reduce its oscillations. However, such systems tend to modify the dynamical characteristics of the overall structure. More importantly, if

*Corresponding author

Email address: simon.charlemagne@entpe.fr (S. Charlemagne)

the frequency to which the TMD is tuned is to change, because of damaging or aging of the main system for example, this device becomes less efficient. To overcome this drawback, a consequent research effort has focused on using nonlinear systems [2, 3, 4, 5, 6, 7], among which the Nonlinear Energy Sink [8, 9, 10, 11, 12, 13, 14, 15] is one of the most popular. Its lack of linear natural frequency enables it to enter in resonance with any frequency and to generate a passive control for large frequency ranges.

Other studies considered multiple-degree-of-freedom (dof) nonlinear attachments. It has been proved that several NES coupled in parallel are able to mitigate effectively energy in addition to providing a better mass distribution over the main structure. Moreover, sets of three NES in series have been showing the capacity to extract energy from several modes simultaneously under impulsive excitation of the primary system [16, 17, 18], whereas a single-dof NES can only engage in sequential resonance captures known as resonance capture cascades [19, 20].

The present paper aims to describe the dynamics of a chain of nonlinear oscillators coupled to a harmonically forced linear system. The study of oscillatory chains can be led in the frame of different concepts. Nonlinear normal modes (NNM) are for instance useful to investigate stationary behaviors or transient resonance captures as it is the case in [16, 17, 18]. In the meantime, the framework of limiting phase trajectories (LPT) has proven recently to be very relevant to describe in weakly damped systems non-stationary processes such as strong energy exchanges or energy localization [21, 22]. Nonetheless, to the authors' best knowledge, the latter approaches have considered so far the oscillatory chain from the discrete point of view. The present work seeks to present a continuous modelling of the chain and study its dynamics via a complexification-averaging method leading to the detection of an invariant manifold. It is the continuation of a previous paper where a discrete analytical approach was used to predict the dynamics of a similar system [23]. Here, the main focus is set on the methodology investigating the chain behaviors thanks to a continuous approximation, all other hypotheses being equal. It leads to a more straightforward treatment by transforming sets of discrete equations into a partial differential equation from which closed-form solutions can be derived.

The paper is organized as follows. A general analytical methodology is detailed in Sect. 2. It is then applied to a system featuring a linear structure coupled to a nonlinear chain with nonlinear on-site potentials in Sect. 3. Finally, conclusions are given in Sect. 4.

2. General methodology

2.1. System modeling

The system considered consists of a forced single-dof linear main system (LMS), with the mass 1 and the displacement v, coupled to a discrete chain of $L+1$ oscillators of mass ϵ ($0 < \epsilon \ll 1$) presenting nonlinear potentials, with the displacements u_j, $j = 1, \dots, L+1$. Governing equations read:

$$\begin{cases} \ddot{v} + \underbrace{\omega_0^2 v + \epsilon g_1(v, \dot{v})}_{\text{LMS}} + \underbrace{\epsilon h_1(v, u_1, \dot{v}, \dot{u}_1)}_{\text{LMS-chain coupling}} = \underbrace{\epsilon f \sin(\omega t)}_{\text{Forcing term}} + \mathcal{O}(\epsilon^2) \\ \ddot{u_1} - \underbrace{h_1(v, u_1, \dot{v}, \dot{u}_1)}_{\text{LMS-chain coupling}} + h_2(u_1, u_2, \dot{u}_1, \dot{u}_2) = \mathcal{O}(\epsilon) \\ \ddot{u}_j + \underbrace{h_c(u_{j-1}, u_j, u_{j+1}, \dot{u}_{j-1}, \dot{u}_j, \dot{u}_{j+1})}_{\text{Chain}} = \mathcal{O}(\epsilon) \quad j = 2, \dots, L \\ \ddot{u}_{L+1} + h_L(u_L, u_{L+1}, \dot{u}_L, \dot{u}_{L+1}) = \mathcal{O}(\epsilon) \end{cases} \tag{1}$$

where g_1 is a linear operator, h_2, h_c and h_L are nonlinear and h_1 can be either linear or nonlinear. Furthermore, the LMS is supposed to be excited around its resonance: $\omega^2 = \omega_0^2(1 + \sigma\epsilon)$, where ω_0 is the angular frequency of the main system and σ plays the role of a detuning parameter.
Considering a high number of nonlinear oscillators, i.e. $L \gg 1$, the continuous limit can be applied to the chain. Its behavior is now described by a continuous function $u(x,t)$ defined as follows:

$$\begin{array}{l} u_j(t) = u(x = j-1, t) \\ x \in [0, L] \end{array} \tag{2}$$

where L is the length of the chain. Such transformation enables to perform Taylor expansions as follows:

$$\begin{array}{rcl} u_{j\pm1} & \approx & u(j-1,t) \pm \dfrac{\partial u}{\partial x}(j-1,t) + \dfrac{1}{2!}\dfrac{\partial^2 u}{\partial x^2}(j-1,t) \pm \dots \\ & & \pm \dfrac{1}{n!}\dfrac{\partial^n u}{\partial x^n}(j-1,t) \dots \end{array} \tag{3}$$

Equation (1) is then turned into a system of four equations. The first one is relative to the LMS and the last three equations form a boundary value

problem: second and last equation stand as the left and right boundary conditions in $x = 0$ and $x = L$ while the third one is a partial differential equation ruling the dynamics of the chain.
We now introduce complex variables of Manevitch [24] ($i = \sqrt{-1}$):

$$\begin{cases} \psi(t)e^{i\omega t} = \dfrac{\partial v(t)}{\partial t} + i\omega v(t) \\ \\ \varphi(x,t)e^{i\omega t} = \dfrac{\partial u(x,t)}{\partial t} + i\omega u(x,t) \end{cases} \tag{4}$$

Those variables are the slow modulation of fast oscillations at the frequency ω.
Time is then embedded to fast (τ_0) and slow (τ_k, $k = 1, 2, \ldots$) time scales [25] connected to each other by the mass ratio ϵ:

$$\tau_0 = t \quad ; \quad \tau_k = \epsilon^k t \quad k = 1, 2, \ldots \tag{5}$$

Those time scales are used to redefine the derivation operator:

$$\frac{d.}{dt} = \frac{\partial .}{\partial \tau_0} + \epsilon \frac{\partial .}{\partial \tau_1} + \epsilon^2 \frac{\partial .}{\partial \tau_2} + \ldots \tag{6}$$

A Galerkin technique is implemented to truncate high harmonics $k\omega$, $k > 1$. For an arbitrary function $s(\tau_0, \tau_1, \tau_2, \ldots)$, it reads:

$$S = \frac{\omega}{2\pi} \int_0^{\frac{2\pi}{\omega}} s(\tau_0, \tau_1, \tau_2, \ldots) e^{-i\omega\tau_0} d\tau_0 \tag{7}$$

As slow modulation variables, ψ and φ are assumed to be independent of τ_0 when applying (7) in the case where ψ, ψ^*, φ or φ^* appear in s. This assumption will be verified a posteriori during the multiple scale expansions or by assuming that asymptotic state is reached after a long enough time τ_0. Injecting Eqs. (2), (4) and (7) into system (1), following system is obtained

(dependence on time is omitted in equations for the sake of brevity):

$$\begin{cases} \dfrac{d\psi}{dt} + \dfrac{i}{2}\left(\omega - \dfrac{\omega_0^2}{\omega}\right)\psi + \epsilon G_1(\psi) + \epsilon H_1(\psi, \varphi(0)) = \dfrac{\epsilon f}{2i} + \mathcal{O}(\epsilon^2) \\ \dfrac{\partial \varphi}{\partial t}(0) + \dfrac{i\omega}{2}\varphi(0) - H_1(\psi, \varphi(0)) + H_2(\varphi(0), \varphi_x(0)) = \mathcal{O}(\epsilon) \\ \dfrac{\partial \varphi}{\partial t}(x) + \dfrac{i\omega}{2}\varphi(x) + H_c(\varphi(x), \varphi_x(x), \varphi_{xx}(x)) = \mathcal{O}(\epsilon) \qquad x \in]0, L[\\ \dfrac{\partial \varphi}{\partial t}(L) + \dfrac{i\omega}{2}\varphi(L) + H_L(\varphi(L), \varphi_x(L)) = \mathcal{O}(\epsilon) \end{cases} \tag{8}$$

where the x subscript stands for the derivation with respect to the space variable. This system shelters multi-scale behaviors that can be traced by deriving equations at successive orders of ϵ.

2.2. Multi-scale behaviors

2.2.1. Fast time scale τ_0

To study the system dynamics at fast time scale, we derive Eq. (8) at the ϵ^0 order.
First equation leads to $\dfrac{\partial \psi}{\partial \tau_0} = 0$, meaning that the amplitude of oscillation of the LMS will vary slowly as a function of the slow time scale τ_1, which is in agreement with the hypothesis made above. The assumption of independency of φ on fast time scale is verified by searching for fixed points of the three remaining equations, i.e. points verifying $\lim\limits_{\tau_0 \to +\infty} \dfrac{\partial \phi(x)}{\partial \tau_0} = 0$. In doing so, we define the Slow Invariant Manifold (SIM) of the system:

$$\begin{cases} \omega_0 \phi(0) + 2i\left[H_1(\psi, \phi(0)) - H_2(\phi(0), \phi_x(0))\right] = 0 \\ \omega_0 \phi(x) - 2i H_c(\phi(x), \phi_x(x), \phi_{xx}(x)) = 0 \qquad x \in]0, L[\\ \omega_0 \phi(L) - 2i H_L(\phi(L), \phi_x(L)) = 0 \end{cases} \tag{9}$$

In previous works studying NES or chains of oscillators for purposes of passive control (see for example [11, 12, 26] for the former and [23] for the latter), the SIM has a discrete structure taking the form of a system of P complex

equations where P is the number of dof of the coupled nonlinear system. Here it is turned in a boundary value problem consisiting of an ordinary differential equation (ODE) and two boundary conditions in $x = 0$ and $x = L$, no matter the number of added oscillators. It depicts the whole range of asymptotic behaviors that the system could face under the assumption that the response is monochromatic. Once solved, an expression of $\phi(x)$ as function of ψ is obtained. Varying ψ enables to describe the various behaviors of the chain at τ_1 time scale. Nonetheless, one needs to study the system equations at slow time scale to predict amplitudes of both the LMS and the chain at its equilibrium and singular points.

2.2.2. Slow time scale τ_1

Considering first equation of system (8) around the SIM, and deriving it at the ϵ^1 order, we obtain an equation describing the variation of main system's envelope at slow time scale:

$$\frac{\partial \psi}{\partial \tau_1} + \frac{i\sigma\omega_0}{2}\psi + G_1(\psi) + H_1(\psi, \phi(0)) = \frac{f}{2i} \tag{10}$$

Besides, we assume that the left boundary condition of the SIM gives the following explicit expression of ψ:

$$\psi = F_l(N(0))e^{i\delta(0)} \tag{11}$$

where $N(x)$ and $\delta(x)$ are the magnitude and the phase of $\phi(x)$, i.e. $\phi(x) = N(x)e^{i\delta(x)}$. Combining Eqs. (10) and (11), a system of the following form can be obtained ($N_0 = N(0)$ and $\delta_0 = \delta(0)$):

$$\begin{cases} \dfrac{\partial N_0}{\partial \tau_1} = \dfrac{f_1(N_0, \delta_0)}{g(N_0, \delta_0)} \\ \\ \dfrac{\partial \delta_0}{\partial \tau_1} = \dfrac{f_2(N_0, \delta_0)}{g(N_0, \delta_0)} \end{cases} \tag{12}$$

Equilibrium and singular points, characterizing periodic regimes and Strongly Modulated Responses (SMR) [27], respectively, can be detected via Eq. (12). Equilibrium points verify $f_1 = f_2 = 0$ and $g \neq 0$, while singular points verify $f_1 = f_2 = g = 0$. Besides, system (12) can be used to plot phase portraits around equilibrium points in order to determine their stability. Those two

equations along with the SIM form a reduced-order model of the overall system. Detection of equilibrium and singular points enables to predict the dynamics of the system and thus design the chain as a passive controller.

3. Example of application: nonlinear chain with local potentials

Let us now consider, as an example of application, the following system (see Fig. 1): a linear oscillator with the mass M, stiffness K and damping C, subjected to external solicitation $F(t)$, is coupled to a chain of nonlinear oscillators of mass $m = \epsilon M$. Connection between each mass of the chain is performed via linear springs of stiffness $\tilde{B}$ and viscous damping Γ. Furthermore, they present local nonlinear restoring forces as $\tilde{V}$.

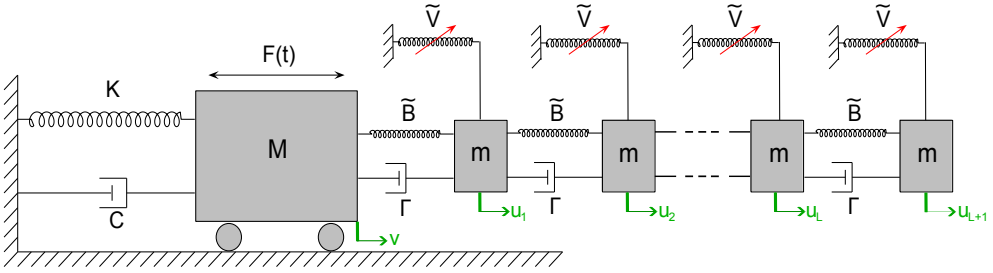

Figure 1: $(L+2)$ dof system consisting of a forced linear structure coupled to $(L+1)$ light nonlinear oscillators ($m = \epsilon M$, $0 < \epsilon \ll 1$).

Governing system equations read:

$$\begin{cases} \ddot{v} + \epsilon c\dot{v} + \omega_0^2 v + \epsilon\gamma(\dot{v} - \dot{u}_1) + \epsilon B(v - u_1) = \epsilon f \sin(\omega t) \\ \ddot{u}_1 + \gamma(-\dot{v} + 2\dot{u}_1 - \dot{u}_2) + B(-v + 2u_1 - u_2) + Du_1^3 = 0 \\ \qquad\qquad \vdots \\ \ddot{u}_j + \gamma(-\dot{u}_{j-1} + 2\dot{u}_j - \dot{u}_{j+1}) + B(-u_{j-1} + 2u_j - u_{j+1}) + Du_j^3 = 0 \\ j = 2, \ldots, L \\ \qquad\qquad \vdots \\ \ddot{u}_{L+1} + \gamma(\dot{u}_{L+1} - \dot{u}_L) + B(u_{L+1} - u_L) + Du_{L+1}^3 = 0 \end{cases} \tag{13}$$

where $\dfrac{K}{M} = \omega_0^2$, $\dfrac{\tilde{B}}{M} = \epsilon B$, $\dfrac{\tilde{V}(z)}{M} = \epsilon D z^3$, $\dfrac{C}{M} = \epsilon c$, $\dfrac{\Gamma}{M} = \epsilon\gamma$, $\dfrac{F(t)}{M} = \epsilon f \sin(\omega t)$ and $\omega^2 = \omega_0^2(1 + \sigma\epsilon)$. This system has the same form as Eq. (1). Hence we can use the method described in Sect. 2.

3.1. SIM of the system: preliminary treatments

Implementing the tools given in Sect. 2 leads to the following definition of the SIM:

$$\begin{cases} \omega_0\phi(0) - \left(i\gamma + \dfrac{B}{\omega_0}\right)\left(-\psi + \phi(0) - \dfrac{\partial\phi}{\partial x}(0)\right) - 2\mathcal{D}|\phi(0)|^2\phi(0) = 0 \\ \omega_0\phi(x) + \left(i\gamma + \dfrac{B}{\omega_0}\right)\dfrac{\partial^2\phi}{\partial x^2}(x) - 2\mathcal{D}|\phi(x)|^2\phi(x) = 0 \qquad x \in]0, L[\\ \omega_0\phi(L) - \left(i\gamma + \dfrac{B}{\omega_0}\right)\dfrac{\partial\phi}{\partial x}(L) - 2\mathcal{D}|\phi(L)|^2\phi(L) = 0 \end{cases} \tag{14}$$

where $\mathcal{D} = \dfrac{3D}{8\omega_0^3}$.

We search solutions under the form $\phi(x) = N(x)e^{i\delta(x)}$. Separating the middle equation of Eq. (14), i.e. the ODE, in real and imaginary parts gives:

$$\omega_0 N + \frac{B}{\omega_0}\left(N_{xx} - N\theta^2\right) - \gamma\left(2N_x\theta + N\theta_x\right) - 2\mathcal{D}N^3 = 0 \tag{15}$$

$$\frac{B}{\omega_0}\left(2N_x\theta + N\theta_x\right) + \gamma\left(N_{xx} - N\theta^2\right) = 0 \tag{16}$$

where $\theta(x) = \delta_x(x)$. We set $\gamma = 0$, which is equivalent to consider an ϵ^2 order damping in the chain, i.e. $\gamma = O(\epsilon)$. Second equation of Eq. (14) then suggests an underlying Hamiltonian that is perturbed by boundary conditions. The framework of LPT or techniques very recently endowed by Gendelman and Sapsis [28] and used for instance in [29] have not been generalized to this study. Equation (16) can now be integrated, leading to:

$$\theta(x) = \frac{\Theta}{N(x)^2} \tag{17}$$

where Θ is a constant of integration. Two remarks can be made:

- if $\exists x_0, N(x_0) = 0$, then $\theta = \delta_x$ presents a singularity in x_0. In other words, whatever the value of Θ may be, a jump in phase is expected in the chain if amplitude is null.

- $N(x)$ is the magnitude of ϕ, so it is positive. However, in the solving process, negative solutions can arise. In this case, the absolute value of the obtained expression of N has to be considered. Then, in order to keep consistency of the solution with the equations, we will add π to the phase $\delta(x)$ at points where $N(x)$ is negative, which is in agreement with the previous remark.

Using Eq. (17), Eq. (15) can be integrated by multiplying by N_x and gives the following relation:

$$N_x^2 = -\frac{\Theta}{N^2} - \frac{\omega_0^2}{B}N^2 + \frac{\mathcal{D}\omega_0}{B}N^4 + C_1 \tag{18}$$

where C_1 is another constant of integration. Θ and C_1 can be determined by using the boundary conditions. Injecting Eqs. (17) and (18) into the last equation of Eq. (14), we obtain:

$$\begin{cases} -\omega_0 N(L) + \dfrac{B}{\omega_0}N_x(L) + 2\mathcal{D}N(L)^3 = 0 \\ N(L)\theta(L) = \dfrac{\Theta}{N(L)} = 0 \end{cases} \tag{19}$$

Equation (19) implies that:

- $\Theta = 0$ (see second equation). Consequently, the phase is constant through the chain, unless there exists one or more points where $N(x) = 0$. At those points, corresponding to a change of sign of $N(x)$, the phase should face a sudden jump of π as previously explained. This means that admissible behaviors of the chain at slow time scale are synchronous periodic oscillations, i.e. NNM according to the definition of Rosenberg [30, 31, 32]. It has already been proven in [23] for a chain with nonlinear next-neighbor coupling that frequency-amplitude dependency of nonlinear modes enables the LMS to solicitate different NNM of the chain depending on the energy injected in the system.

- The first equation stands as the right boundary condition expressing the amplitude of the last mass of the chain.

- If $N(L) = 0$, then $N_x(L) = 0$ (see first equation) and $C_1 = 0$ (see Eq. (18)). Yet, when $C_1 = 0$, expression of N_x^2 is strictly positive iff

$N(x) > \sqrt{\frac{\omega_0}{\mathcal{D}}}$, which does not allow $N(L) = 0$. As a consequence, if $N(L) = 0$, then $\forall x, N(x) = 0$. We will from now on focus on nontrivial solutions, corresponding to the case $C_1 \neq 0$.

Now injecting Eq. (17) into the first equation of Eq. (14), we obtain:

$$\begin{cases} \left(\frac{B}{\omega_0} - \omega_0 + 2\mathcal{D}N(0)^2\right) N(0) - \frac{B}{\omega_0} N_x(0) = \frac{B}{\omega_0} N_1 \cos(\delta_1 - \delta(0)) \\ \\ N_1 \sin(\delta_1 - \delta(0)) = 0 \end{cases} \tag{20}$$

where $\psi = N_1 e^{i\delta_1}$. The second equation shows that the LMS oscillates either in phase or in opposite phase with the first mass of the chain: $\delta_1 = \delta_0 + k\pi, k = 0, 1$. First equation then becomes:

$$N_1 = \pm \left[\left(1 - \frac{\omega_0^2}{B} + 2\frac{\omega_0 \mathcal{D}}{B} N(0)^2\right) N(0) - N_x(0) \right] \tag{21}$$

Finally, we obtain the following system of equations to be solved:

$$\begin{cases} N_x^2 = -\frac{\omega_0^2}{B} N^2 + \frac{\mathcal{D}\omega_0}{B} N^4 + C_1 \\ \\ N_1 = \pm \left[\left(1 - \frac{\omega_0^2}{B} + 2\frac{\omega_0 \mathcal{D}}{B} N(0)^2\right) N(0) - N_x(0) \right] \\ \\ -\omega_0 N(L) + \frac{B}{\omega_0} N_x(L) + 2\mathcal{D}N(L)^3 = 0 \end{cases} \tag{22}$$

3.2. Solutions of the equations of the SIM

Let us investigate the ODE, i.e. the first equation of system (22). The constant C_1 plays an important role. Indeed, if it is superior to a critical value $C_{1crit} = \frac{\omega_0^3}{4B\mathcal{D}}$, then the polynomial expression of N_x^2 has no real roots. Otherwise, there exists two real roots X_1 and X_2 defined as follows:

$$\begin{aligned} & N_x = 0 \Leftrightarrow N = \sqrt{X_{1,2}} \\ & X_{1,2} = \frac{\omega_0^2 \pm \sqrt{\omega_0^4 - 4BC_1\mathcal{D}\omega_0}}{2\mathcal{D}\omega_0}, \qquad X_1 < X_2 \end{aligned} \tag{23}$$

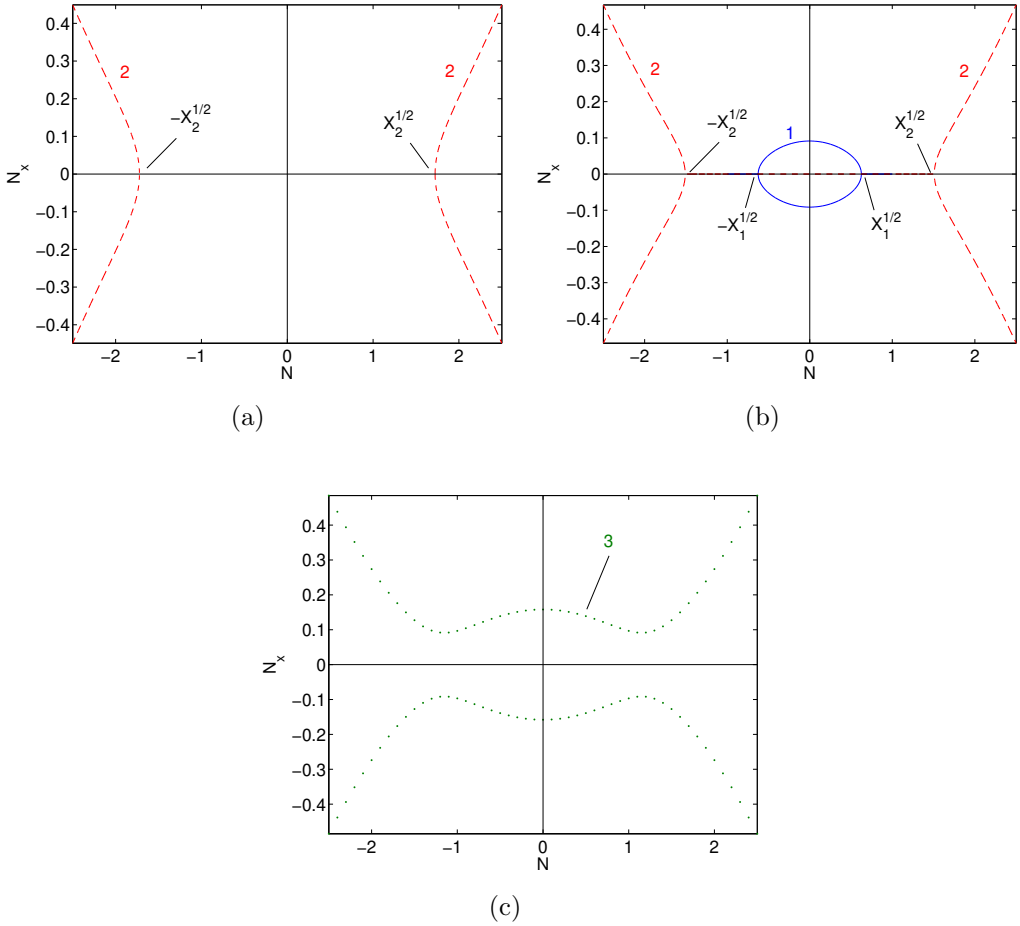

Figure 2: Phase portraits obtained from the first equation of system (22) for the following parameters: $\omega_0 = 1$, $B = 40$, $D = 1$ and (a) $C_1 = -\frac{1}{2}C_{1crit}$ (b) $C_1 = \frac{1}{2}C_{1crit}$ (b) $C_1 = \frac{3}{2}C_{1crit}$. Three possible branches are named as 1, 2 and 3.

Finally, the asymptotic dynamics of the chain can take place along three different "branches" named as 1, 2 and 3, depending on the value of C_1. They are depicted in Fig. 2.
Let us now inject expression of $N_x(L)$ obtained from the ODE into the right boundary condition (last equation of system (22)):

$$\frac{B^2}{\omega_0^2}\left(-\frac{\omega_0^2}{B}N(L)^2 + \tilde{\mathcal{D}}N(L)^4 + C_1\right) - (\omega_0 N(L) - 2\mathcal{D}N(L)^3)^2 = 0 \qquad (24)$$

Because of the symmetry of the phase portraits in Fig. 2, we can focus on positive solutions $N(L)$. This relation has one, two or three real solutions. It has three solutions when:

$$\begin{array}{lll} C_{1crit} < C_1 < C_{1m} & \text{if} & B < 2\omega_0^2 \\ C_{1m} < C_1 < C_{1crit} & \text{if} & B > 2\omega_0^2 \end{array} \tag{25}$$

where $C_{1m} = \dfrac{(8\omega_0^2 - B)(B + \omega_0^2)^2}{108B^2\mathcal{D}\omega_0}$. If $B = 2\omega_0^2$, then $C_{1m} = C_{1crit}$ and Eq. (24) has one real solution. Values of solutions of Eq. (24) are plotted in Fig. 3, with line styles and colors corresponding to the ones used in Fig. 2 so that one can relate the different values of $N(L)$ to the branches 1, 2 or 3 and the corresponding operating ranges. Value of the parameter B is chosen different from Fig. 2 for the sake of clarity of Fig. 3. For each value of $N(L)$,

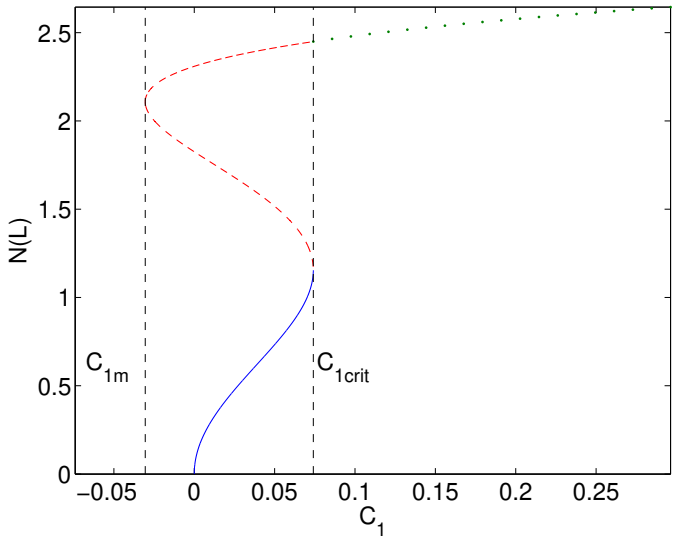

Figure 3: $\omega_0 = 1$, $B = 9$ and $D = 1$ – Plot of the solutions of Eq. (24). Line styles correspond to cases described in Fig. 2.

starting from 0 and progressing along this curve, we aim to integrate the first equation of system (22), thus obtaining $N(0)$ and $N_x(0)$ and eventually N_1 through the left boundary condition (second equation of system (22)). This procedure will permit to plot the projection of the SIM in the $(N(L), N_1)$ plane.

Let us first focus on branch 1, i.e. the case where $C_1 < C_{1crit}$ and $N(x) < \sqrt{X_1}$. Then expression of N_x^2 can be rewritten as:

$$N_x = \pm\sqrt{\tilde{\mathcal{D}}(X_1 - N^2)(X_2 - N^2)} \tag{26}$$

where $\tilde{\mathcal{D}} = \dfrac{\mathcal{D}\omega_0}{B}$. Integration of Eq. (26) leads to:

$$N(x) = \sqrt{X_1}\,\mathrm{sn}\left(\sqrt{\frac{C_1}{X_1}}(x - C_2), \frac{X_1}{X_2}\right) \tag{27}$$

where $\mathrm{sn}(X, k^2)$ is a Jacobian elliptic function and C_2 a constant of integration which can be determined through the following expression:

$$C_2 = L - \sqrt{\frac{X_1}{C_1}}\,\mathrm{F}\left(\arcsin\left(\frac{N(L)}{\sqrt{X_1}}\right), \frac{X_1}{X_2}\right) \tag{28}$$

where $\mathrm{F}(X, k^2)$ is the incomplete elliptic integral of the first kind. Equation (27) gives an explicit expression of the modal shapes of the NNM of the chain that are able to enter in resonance with the frequency of the LMS. The part of the SIM stemming from branch 1 is plotted in Fig. 4 in blue solid line for the following parameters: $\omega_0 = 1$, $B = 40$, $D = 1$ and $L = 30$. In order to continue this plot, one needs to integrate the ODE for higher values of $N(L)$ corresponding to branches 2 and 3. However, there is no closed-form expression of $N(x)$ on those branches. As a result, one needs to numerically integrate the following expression:

$$dx = \pm\frac{dN}{\sqrt{-\dfrac{\omega_0^2}{B}N^2 + \dfrac{\mathcal{D}\omega_0}{B}N^4 + C_1}} \tag{29}$$

It can be proven that such integration leads to detection of a monotonic increasing branch of the SIM plotted in Fig. 4 (red dotted line).

3.3. Equilibrium and singular points

The equation relative to the LMS around the SIM derived at the ϵ^1 order reads:

$$\frac{\partial\psi}{\partial\tau_1} + \frac{1}{2}\left(c\psi + i\sigma\omega_0 - \frac{iB}{\omega_0}\right)\psi + \frac{iB}{\omega_0}\phi(0) = \frac{f}{2i} \tag{30}$$

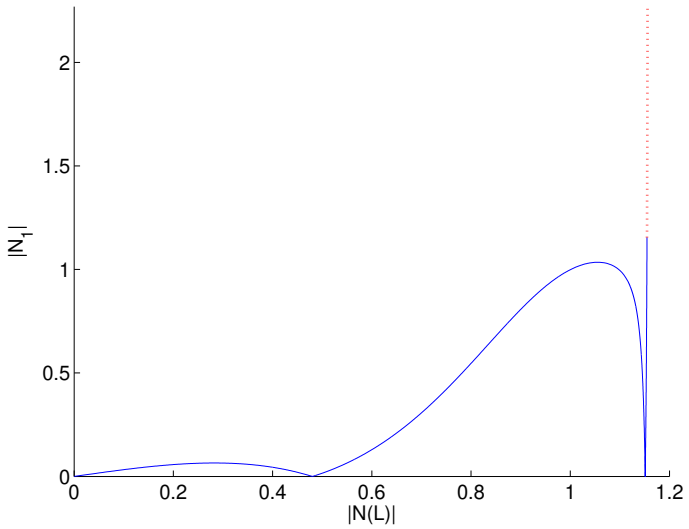

Figure 4: $L = 30$, $\omega_0 = 1$, $B = 40$ and $D = 1$ – Example of SIM. Line styles correspond to cases described in Fig. 2.

Left boundary condition of the SIM gives:

$$\begin{aligned} &\psi = F_l(N_0)e^{i\delta_0} \\ &F_l(N_0) = -N_x(0) + \left(1 - \frac{\omega_0^2}{B} + 2\tilde{\mathcal{D}}N_0^2\right) N_0 \end{aligned} \tag{31}$$

Injecting Eq. (31) into Eq. (30), we obtain:

$$\begin{cases} \dfrac{\partial N_0}{\partial \tau_1} = \dfrac{f_1(N_0, \delta_0)}{g(N_0)} \\ \dfrac{\partial \delta_0}{\partial \tau_1} = \dfrac{f_2(N_0, \delta_0)}{g(N_0)} \end{cases} \tag{32}$$

where

$$\begin{cases} f_1(N_0, \delta_0) = -\dfrac{F_l(N_0)}{2}\left[cF_l(N_0) + f\sin(\delta_0)\right] \\ f_2(N_0, \delta_0) = \dfrac{1}{2}\dfrac{\partial F_l(N_0)}{\partial N_0}\left[\left(\dfrac{B}{\omega_0} - \sigma\omega_0\right)F_l(N_0) - \dfrac{B}{\omega_0}N_0 - f\cos(\delta_0)\right] \\ g(N_0) = F_l(N_0)\dfrac{\partial F_l(N_0)}{\partial N_0} \end{cases} \tag{33}$$

$g(N_0) = 0$ gives points of the SIM where singular points can appear. They are located on the local extremums in Fig. 4: $F_l(N_0) = 0$ corresponds to the minimums ($N_1 = 0$) and $\dfrac{\partial F_l(N_0)}{\partial N_0}$ to the maximums. We introduce variables $N_{0,min}^{(k)}$ and $N_{0,max}^{(k)}$, where k denotes the number of local maximums (or minimums), defined as follows: $F_l(N_{0,min}^{(k)}) = 0$ and $\dfrac{\partial F_l(N_{0,max}^{(k)})}{\partial N_0} = 0$. To detect singular points, one should also verify the condition $f_1(N_0, \delta_0) = f_2(N_0, \delta_0) = 0$, which comes down to:

$$\begin{aligned} &\cos(\delta_0) = -\frac{BN_{0,min}^{(k)}}{f\omega_0} \\ &\text{or} \\ &\sin(\delta_0) = -\frac{cF_l(N_{0,max}^{(k)})}{f} \end{aligned} \tag{34}$$

As $|\cos(\delta_0)|$ and $|\sin(\delta_0)|$ are bounded, it is possible to define critical values of the forcing amplitude above which singular points arise at the corresponding values of $N(0)$, i.e. at the corresponding local extremums of the SIM:

$$\begin{aligned} f_{crit,min}^{(k)} &= \left| \frac{BN_{0,min}^{(k)}}{\omega_0} \right| \\ f_{crit,max}^{(k)} &= \left| cF_l(N_{0,max}^{(k)}) \right| \end{aligned} \tag{35}$$

Despite the complexity of the initial system, the method of detection of equilibrium and singular points is straightforward compared to the procedure used in [23]. Besides, it enables to detect critical forcing amplitudes of Eq. (35) which can be of great use when trying to design the chain as a passive controller. Analytical predictions are now to be compared to numerical results which take into account the real discrete behavior of the overall system.

3.4. Numerical results

3.4.1. Validation of analytical predictions

In this section, numerical simulations obtained from time integration of system (13), i.e. the initial discrete system of equations, are confronted with

analytical predictions of Sects. 3.1, 3.2 and 3.3. Integration is performed thanks to the *ode45* function of Matlab (Runge-Kutta scheme), with following options: time step of 0.1, absolute and relative error tolerances of 10^{-12}. At initial time, all masses of the system are at rest. From the physical amplitudes obtained, i.e. $v(t)$ and $u_j(t), j = 1, \ldots, L+1$, we can compute ψ and the discrete equivalent of $\varphi(x,t)$, which is a $(L+1)$ vector constituted of the variables:

$$\varphi_{j+1}(t) = (\dot{u}_j(t) + i\omega u_j(t))\, e^{-i\omega t} = N_{j+1}(t) e^{i\delta_{j+1}(t)} \tag{36}$$

Let us first set $L = 30$, $\epsilon = 0.001$, $\omega_0 = 1$, $B = 100$, $D = 1$, $c = 0.5$, $f = 0.5$ and $\sigma = 0$. A small damping $\gamma = 0.1$ is also added in numerical simulations. The SIM and its equilibrium and singular points are depicted in Fig. 5(a). The system has one equilibrium point on its first branch. The phase portrait in Fig. 5(b) shows that it is stable. A singular point is also present on the local maximum as $f^{(1)}_{crit,max} = 0.340 < f < f^{(1)}_{crit,min} = 8.370$. Thus, after a quick transient state, the system behavior is expected to be attracted by the SIM and either stabilize around the equilibrium point or face SMR driven by the singular point. It can be seen on Fig. 6 that the system reaches an

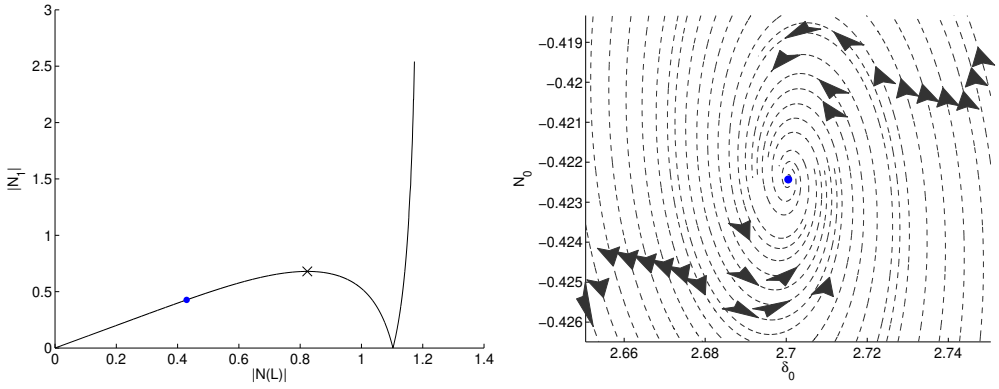

(a) (b)

Figure 5: $L = 30$, $\epsilon = 0.001$, $\omega_0 = 1$, $B = 100$, $D = 1$, $c = 0.5$, $f = 0.5$ and $\sigma = 0$ – (a) SIM of the system (black line) with equilibrium and singular points (blue point and black cross, respectively) (b) Phase portrait around the equilibrium point

equilibrium state. However, there is a significant discrepancy between the final amplitudes of the system and the prediction (see blue and red points in Fig. 6(b)). This difference comes from the transition to the continuum limit,

which can be seen in Fig. 7(a) where blue triangles depict the prediction of final amplitudes of each oscillator of the chain obtained from the discrete approach used in [23]. This prediction fits numerical amplitudes represented by red crosses. Nonetheless, SIM obtained from both methods, plotted side to side in Fig. 7(b), are in good agreement. Analytical results also succeed to predict correctly the general behavior of the system: the blue solid line in Fig. 7(a) reaches 0 at $x = 14.4$. It means that during the steady-state regime, the chain should present two groups of particles oscillating in opposite phase with the middle oscillators (no. 14 and 15) having a near-zero amplitude, which is validated by the numerical results in Fig. 8. Finally, the discrepancies between predictions of continuous and discrete approaches decrease as the length of the chain increases. Increasing this length to $L = 50$ and setting $f = 2$, all other things being equal, five equilibrium points are detected. Comparisons of predicted amplitudes of the oscillators of the chain (i.e. N_j or $N(x)$) around equilibrium points obtained from discrete and continuous approaches are given in Fig. 9. They are in good accordance.

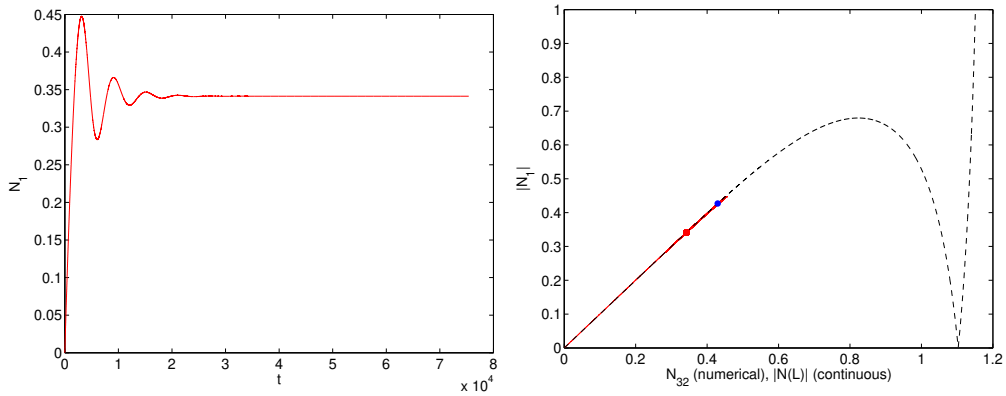

(a) (b)

Figure 6: $L = 30$, $\epsilon = 0.001$, $\omega_0 = 1$, $B = 100$, $D = 1$, $c = 0.5$, $f = 0.5$ and $\sigma = 0$ – (a) N_1 versus time obtained from numerical results (b) SIM of the system (dashed black line) and equilibrium point (blue point) with corresponding numerical results (red line). The red point shows the final amplitudes of the system obtained from numerical results

Changing the forcing parameters to $f = 4.5$ and $\sigma = 10$, three equilibrium points (no. 1, 2 and 3) and a singular point are detected on the SIM, as shown in Fig. 10. Points no. 1 and 2 are unstable while point no. 3 is stable (see

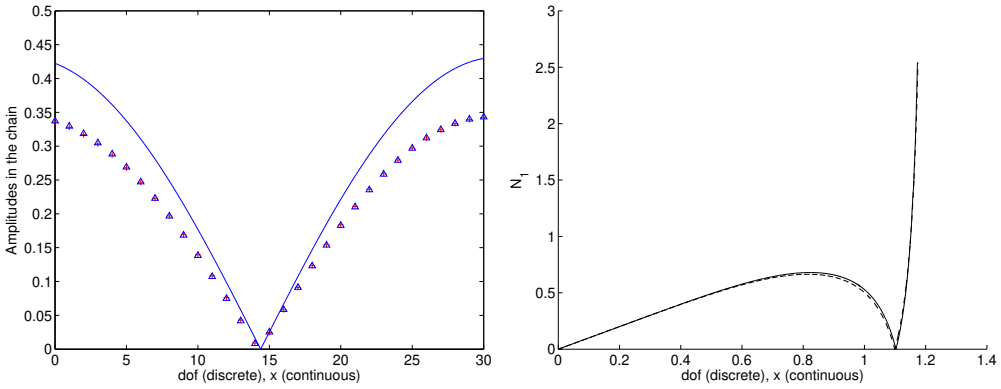

(a) (b)

Figure 7: $L = 30$, $\epsilon = 0.001$, $\omega_0 = 1$, $B = 100$, $D = 1$, $c = 0.5$, $f = 0.5$ and $\sigma = 0$ – (a) Comparison of amplitudes of the masses of the chain obtained from discrete (triangles) and continuous (solid line) approaches and numerical results (red crosses) (b) Comparison of the SIM obtained from discrete (dashed line) and continuous (solid line) approaches

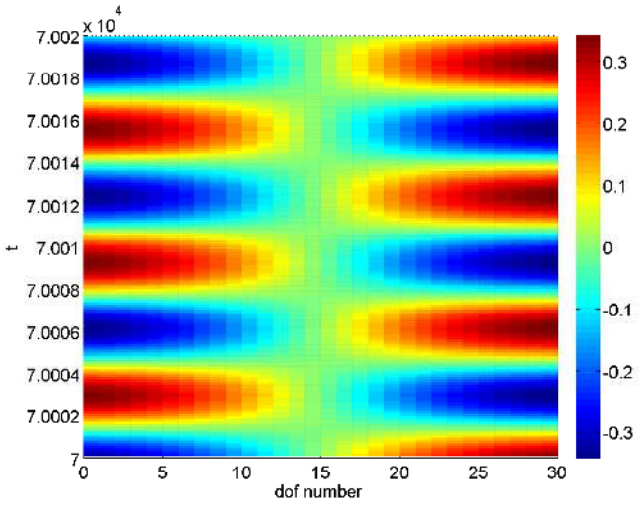

Figure 8: $L = 30$, $\epsilon = 0.001$, $\omega_0 = 1$, $B = 100$, $D = 1$, $c = 0.5$, $f = 0.5$ and $\sigma = 0$ – Evolution of the physical amplitudes of oscillation u_j of each oscillator of the chain obtained from numerical results at τ_1 time scale

phase portraits in Fig. 10(b)-(d)). Numerical results in Fig. 11, for which the damping has been increased to $\gamma = 5$, show that the system faces SMR. Fig. 11(a) depicts the cycle that the system follows repeatedly on the SIM,

bifurcating from one branch to another. During those cycles, a 1:1 resonance is engaged between two NNM of the chain which are caught in an intense energy exchange regime. Figure 12 plots a bifurcation between the NNM excited on the lower branch of the SIM and the one solicitated on the higher branch. Such non-stationary behavior ensuing from inter-modal resonance has been observed and predicted within the framework of LPT in different systems such as discrete periodic Klein-Gordon [33] and Fermi-Pasta-Ulam [34] chains.

3.4.2. Evidence of passive control

In this section, an example of passive control of the linear system performed by the chain is shown. We aim to prove that a part of the main structure's vibratory energy can be transferred into the chain, without any consideration about a possible optimal design of the system parameters. To this end, we consider the same set of parameters as in the previous section, i.e. $L = 30$, $\epsilon = 0.001$, $\omega_0 = 1$, $B = 100$, $D = 1$ and $c = 0.5$, and we investigate the existence and amplitudes of equilibrium and singular points when varying the amplitude of external excitation, i.e. f, at the exact resonance with the LMS ($\sigma = 0$). A comparison with the amplitude N_1 that the LMS would have without the presence of the chain is led.
Obtained results for $f \in [0.1, 10]$ is depicted in Fig. 13. Black solid line denotes the amplitudes that the LMS would face without the chain. It is given by the following relation : $N_1 = \dfrac{f}{\sqrt{c^2 + \sigma^2\omega_0^2}} = 2f$. For the sake of clarity, the straight line has been cut. It clearly appears that the LMS has lower amplitudes with the chain, especially at relatively high energies. Nonetheless, around $f = 0.6$, an equilibrium point has the same amplitude as the LMS without the chain. Thus, a parametric study needs to be led to enhance the control performance at low energy. This is out of the scope of this paper.

4. Conclusions

The present work studies the dynamics of a chain of light nonlinear oscillators coupled to a linear structure through a method using the continuous limit to describe the behavior of the chain. It is the continuation of a work using a discrete description with the same hypotheses. A general methodology is presented and applied to an example of a chain with cubic on-site

restoring forces. The slow invariant manifold of the system is defined at fast time scale by a boundary value problem which has a closed-form solution being valid for a large range of amplitudes. At slow time scale, equilibrium and singular points are detected. They predict periodic regimes and strongly modulated responses, respectively. Comparisons with the discrete approach show good agreements when the chain is long enough. This is a predictable result since it is a mandatory assumption for applying the continuous approximation. Confrontation with numerical simulations enables to validate this approach and shows that the method can be used to design nonlinear chains of oscillators for purposes of passive control.

Acknowledgements

The authors would like to thank following organizations for supporting this research: i) The "Ministère de la Transition Écologique et Solidaire" ii) LABEX CELYA (ANR-10-LABX-0060) of the "Université de Lyon" within the program "Investissement d'Avenir" (ANR-11-IDEX-0007) operated by the French National Research Agency (ANR).

References

[1] H. Frahm, Device for damping vibrations of bodies, US 989958.

[2] R. E. Roberson, Synthesis of a nonlinear dynamic vibration absorber, Journal of the Franklin Institute 254 (3) (1952) 205 – 220.

[3] L. A. Pipes, Analysis of a nonlinear dynamic vibration absorber, Journal of Applied Mechanics 20 (1953) 515 – 518.

[4] F. R. Arnold, Steady-state behavior of systems provided with nonlinear dynamic vibration absorbers, Journal of Applied Mechanics 22 (1955) 487 – 492.

[5] J. Hunt, J.-C. Nissen, The broadband dynamic vibration absorber, Journal of Sound and Vibration 83 (4) (1982) 573 – 578.

[6] J. Shaw, S. W. Shaw, A. G. Haddow, On the response of the nonlinear vibration absorber, International Journal of Non-Linear Mechanics 24 (4) (1989) 281 – 293.

[7] O. V. Gendelman, Transition of energy to a nonlinear localized mode in a highly asymmetric system of two oscillators, Nonlinear Dynamics 25 (1) (2001) 237–253.

[8] O. V. Gendelman, L. I. Manevitch, A. F. Vakakis, R. M'Closkey, Energy pumping in nonlinear mechanical oscillators: Part i-dynamics of the underlying hamiltonian systems, Journal of Applied Mechanics 68 (2000) 34–41.

[9] A. F. Vakakis, O. V. Gendelman, Energy pumping in nonlinear mechanical oscillators: part ii-resonance capture, Journal of Applied Mechanics 68 (2000) 42–48.

[10] G. Kerschen, D. M. McFarland, J. J. Kowtko, Y. S. Lee, L. A. Bergman, A. F. Vakakis, Experimental demonstration of transient resonance capture in a system of two coupled oscillators with essential stiffness nonlinearity, Journal of Sound and Vibration 299 (4) (2007) 822 – 838.

[11] O. V. Gendelman, Analytic treatment of a system with a vibro-impact nonlinear energy sink, Journal of Sound and Vibration 331 (2012) 4599–4608.

[12] E. Gourc, G. Michon, S. Seguy, A. Berlioz, Experimental investigation and design optimization of targeted energy transfer under periodic forcing, Journal of Vibration and Acoustics 136 (2014) 021021.

[13] A. Luongo, D. Zulli, Aeroelastic instability analysis of nes-controlled systems via a mixed multiple scale/harmonic balance method, Journal of Vibration and Control 20 (2014) 1985–1998.

[14] J. Shao, B. Cochelin, Theoretical and numerical study of targeted energy transfer inside an acoustic cavity by a non-linear membrane absorber, International Journal of Non-Linear Mechanics 64 (2014) 85–92.

[15] E. Boroson, S. Missoum, P.-O. Mattei, C. Vergez, Optimization under uncertainty of parallel nonlinear energy sinks, Journal of Sound and Vibration 394 (2017) 451–464.

[16] P. N. Panagopoulos, A. F. Vakakis, S. Tsakirtzis, Transient resonant interactions of finite linear chains with essentially nonlinear end attachments leading to passive energy pumping, International Journal of Solids and Structures 41 (2223) (2004) 6505 – 6528.

[17] S. Tsakirtzis, G. Kerschen, P. N. Panagopoulos, A. F. Vakakis, Multi-frequency nonlinear energy transfer from linear oscillators to mdof essentially nonlinear attachments, Journal of Sound and Vibration 285 (12) (2005) 483 – 490.

[18] S. Tsakirtzis, P. N. Panagopoulos, G. Kerschen, O. Gendelman, A. F. Vakakis, L. A. Bergman, Complex dynamics and targeted energy transfer in linear oscillators coupled to multi-degree-of-freedom essentially nonlinear attachments, Nonlinear Dynamics 48 (3) (2007) 285–318.

[19] A. F. Vakakis, L. I. Manevitch, O. V. Gendelman, L. A. Bergman, Dynamics of linear discrete systems connected to local, essentially nonlinear attachments, Journal of Sound and Vibration 264 (3) (2003) 559 – 577.

[20] A. F. Vakakis, D. M. McFarland, L. A. Bergman, L. I. Manevitch, O. V. Gendelman, Isolated resonance captures and resonance capture cascades leading to single- or multi-mode passive energy pumping in damped coupled oscillators, Journal of Vibration and Acoustics 126 (2004) 235–244.

[21] L. Manevitch, New approach to beating phenomenon in coupled nonlinear oscillatory chains, Archive of Applied Mechanics 77 (5) (2007) 301–312.

[22] L. I. Manevitch, V. V. Smirnov, Limiting phase trajectories and the origin of energy localization in nonlinear oscillatory chains, Physical Review E 82 (2010) 036602.

[23] S. Charlemagne, C.-H. Lamarque, A. Ture Savadkoohi, Vibratory control of a linear system by addition of a chain of nonlinear oscillators, Acta Mechanica 228 (9) (2017) 3111–3133.

[24] L. I. Manevitch, The description of localized normal modes in a chain of nonlinear coupled oscillators using complex variables, Nonlinear Dynamics 25 (2001) 95–109.

[25] A. Nayfeh, D. Mook, Nonlinear Oscillations, John Wiley and Sons, 1979.

[26] S. Charlemagne, A. Ture Savadkoohi, C.-H. Lamarque, Interactions between two coupled nonlinear forced systems: Fast/slow dynamics, International Journal of Bifurcation and Chaos 26 (2016) 1650155.

[27] Y. Starosvetsky, O. V. Gendelman, Strongly modulated response in forced 2dof oscillatory system with essential mass and potential asymmetry, Physica D 237 (2008) 1719–1733.

[28] O. V. Gendelman, T. P. Sapsis, Energy exchange and localization in essentially nonlinear oscillatory systems: Canonical formalism, Journal of Applied Mechanics 84 (2017) 011009.

[29] O. V. Gendelman, Escape of a harmonically forced particle from an infinite-range potential well: a transient resonance, Nonlinear Dynamicsdoi:10.1007/s11071-017-3801-x.

[30] R. M. Rosenberg, Normal modes of nonlinear dual-mode systems, Journal of Applied Mechanics 27 (1960) 263–268.

[31] R. M. Rosenberg, The normal modes of nonlinear n-degree-of-freedom systems, Journal of Applied Mechanics 29 (1962) 7–14.

[32] R. M. Rosenberg, On nonlinear vibrations of systems with many degrees of freedom, Advances in Applied Mechanics 9 (1966) 155–242.

[33] V. V. Smirnov, L. I. Manevich, Limiting phase trajectories and dynamic transitions in nonlinear periodic systems, Acoustical Physics 57 (2) (2011) 271–276.

[34] Y. Starosvetsky, L. Manevitch, On intense energy exchange and localization in periodic fpu dimer chains, Physica D: Nonlinear Phenomena 264 (Supplement C) (2013) 66 – 79.

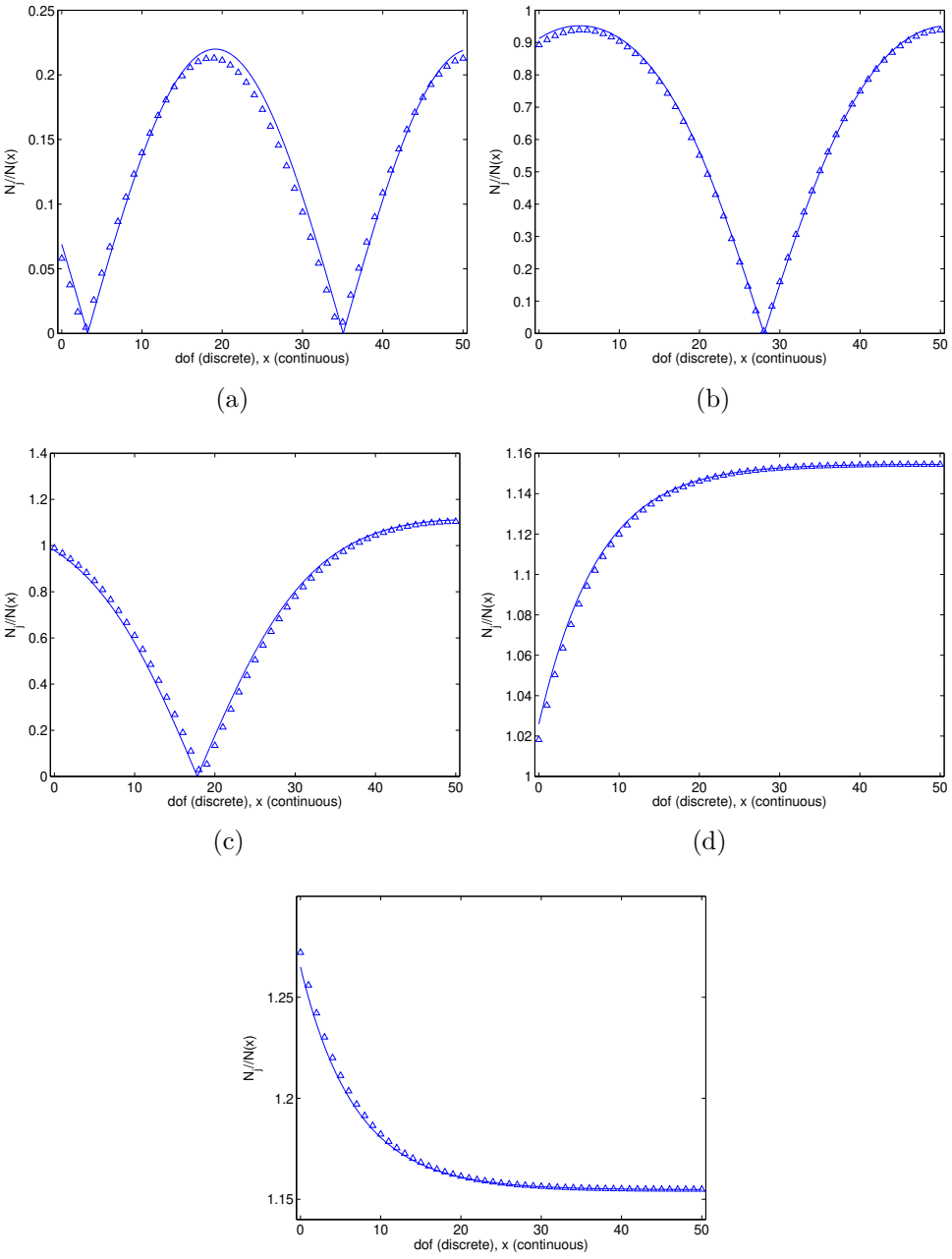

Figure 9: $L = 50$, $\epsilon = 0.001$, $\omega_0 = 1$, $B = 100$, $D = 1$, $c = 0.5$, $f = 2$ and $\sigma = 0$ – Comparisons of predicted amplitudes of the masses of the chain on the five equilibrium points obtained from discrete (triangles) and continuous (solid line) approaches.

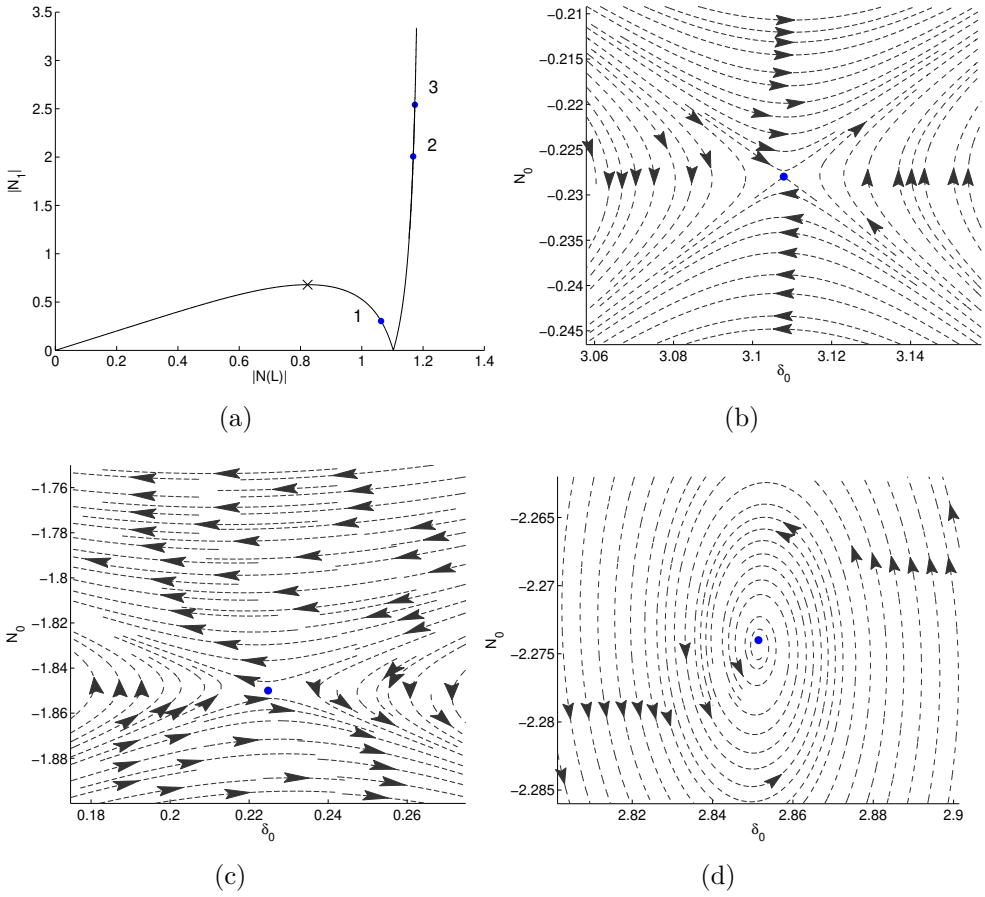

Figure 10: $L = 30$, $\epsilon = 0.001$, $\omega_0 = 1$, $B = 100$, $D = 1$, $c = 0.5$, $f = 4.5$ and $\sigma = 10$ – (a) SIM of the system (black line) with equilibrium and singular points (blue points and black cross, respectively) (b)-(d) Phase portraits around equilibrium points no. 1, 2 and 3, respectively.

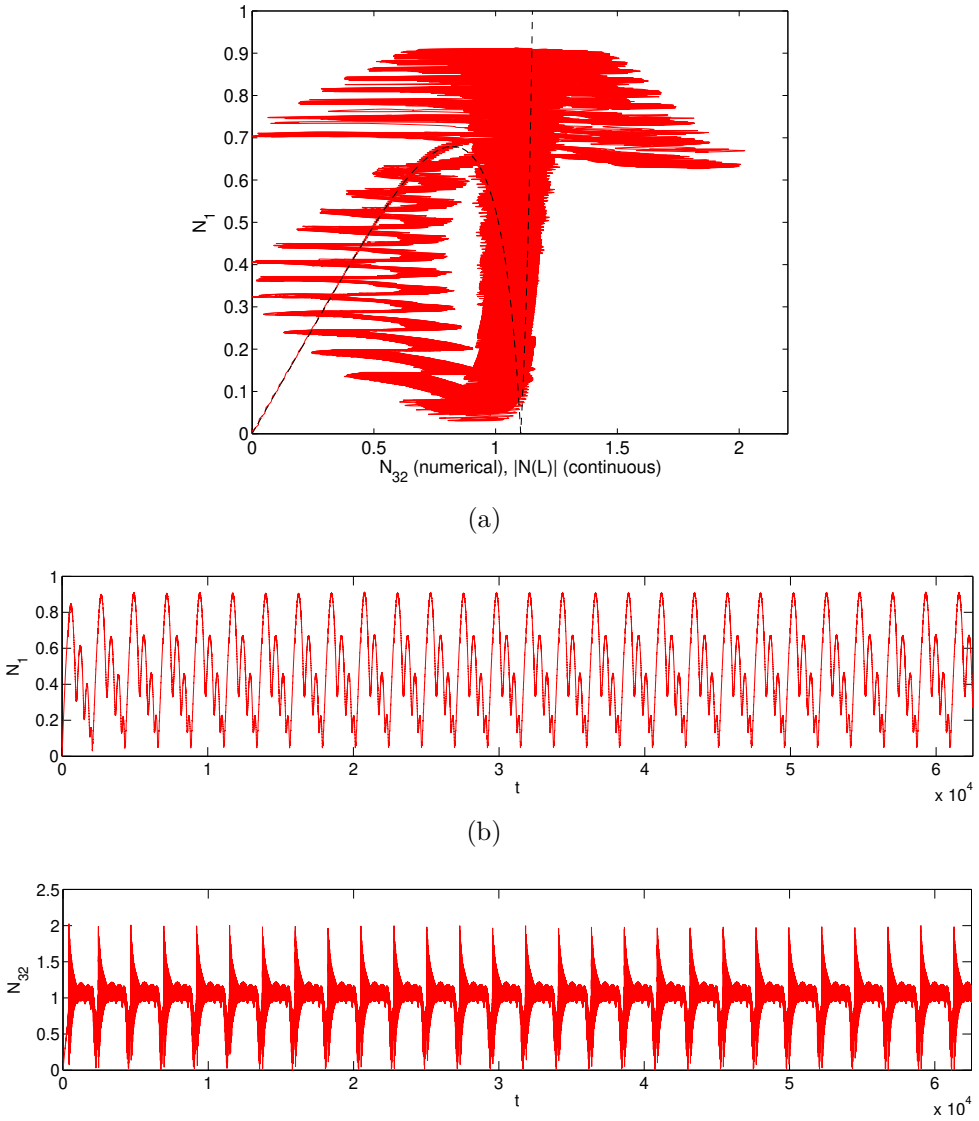

Figure 11: $L = 30$, $\epsilon = 0.001$, $\omega_0 = 1$, $B = 100$, $D = 1$, $c = 0.5$, $f = 4.5$ and $\sigma = 10$ – (a) SIM of the system (dashed black line) with corresponding numerical results (red line) (b) N_1 versus time obtained from numerical results (c) N_{32} versus time obtained from numerical results.

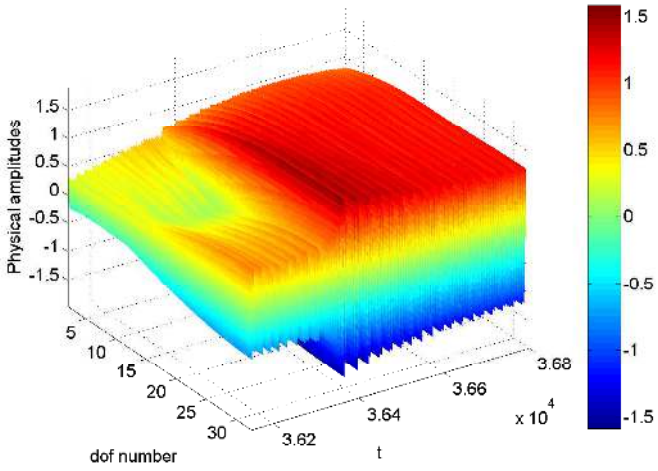

Figure 12: $L = 30$, $\epsilon = 0.001$, $\omega_0 = 1$, $B = 100$, $D = 1$, $c = 0.5$, $f = 4.5$ and $\sigma = 10$ – Evolution of the physical amplitudes of oscillation u_j of each oscillator of the chain obtained from numerical results at τ_1 time scale

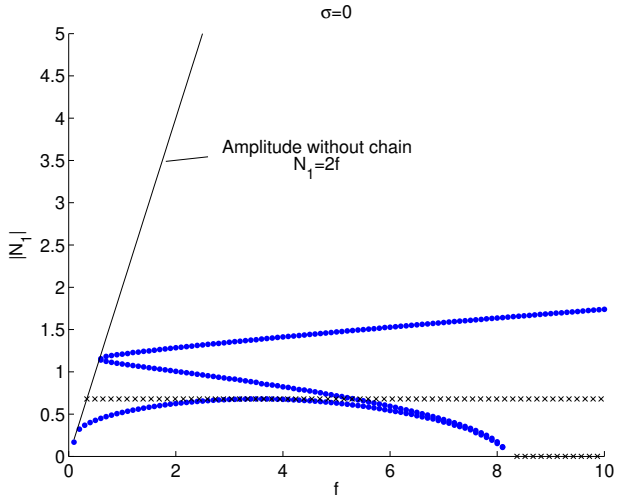

Figure 13: $L = 30$, $\epsilon = 0.001$, $\omega_0 = 1$, $B = 100$, $D = 1$, $c = 0.5$ and $\sigma = 0$ – $|N_1|$-amplitudes of equilibrium and singular points (blue points and black crosses, respectively) of the system when the forcing magnitude f varies. Black solid line denotes the amplitude the LMS would face without the chain.